# Spin-Polarized Positronium Time-of-Flight Spectroscopy for Probing Spin-Polarized Surface Electronic States

M. Maekawa, A. Miyashita, S. Sakai, S. Li, S. Entani, and A. Kawasuso*
*National Institutes for Quantum and Radiological Science and Technology, 1233 Watanuki, Takasaki, Gunma 370-1292, Japan*

Y. Sakuraba
*National Institute for Materials Science (NIMS), 1-2-1, Sengen, Tsukuba-city, Ibaraki 305-0047, Japan*

(Received 5 November 2020; accepted 25 March 2021; published 4 May 2021)

The energy spectrum of positronium atoms generated at a solid surface reflects the electron density of states (DOS) associated solely with the first surface layer. Using spin-polarized positrons, the spin-dependent surface DOS can be studied. For this purpose, we have developed a spin-polarized positronium time-of-flight spectroscopy apparatus based on a $^{22}$Na positron source and an electrostatic beam transportation system, which enables the sampling of topmost surface electrons around the Γ point and near the Fermi level. We applied this technique to nonmagnetic Pt(111) and W(001), ferromagnetic Ni (111), Co(0001) and graphene on them, $Co_2FeGa_{0.5}Ge_{0.5}$ (CFGG) and $Co_2MnSi$ (CMS). The results showed that the electrons of Ni(111) and Co(0001) surfaces have characteristic negative spin polarizations, while these spin polarizations vanished upon graphene deposition, suggesting that the spin polarizations of graphene on Ni(111) and Co(0001) were mainly induced at the Dirac points that were out of range in the present measurement. The CFGG and CMS surfaces also exhibited only weak spin polarizations suggesting that the half-metallicity expected for these bulk states was not maintained at the surfaces.

DOI: 10.1103/PhysRevLett.126.186401

Slow positrons injected into the subsurface region of a metal diffuse back to the surface/vacuum interface and are emitted as positronium (Ps) atoms by picking up the outermost surface electrons when the Ps formation potential is negative. Because of the energy gain of the formation potential, electrons below the Fermi level with the width of formation potential can participate in Ps formation. Hence, Ps energy spectroscopy can provide information regarding the surface electron density of states (DOS) [1]. Although Ps spectroscopy is analogous to photoemission spectroscopy, a critical difference is its extremely high surface sensitivity [2,3]. This owes to the fact that Ps atom is formed only at the top surface of metal [4,5], while the photoemission spectroscopy includes electrons from several surface layers. Recently, the angle-resolved Ps spectroscopy with a milli-electron-volt energy resolution has been demonstrated in a laboratory scale [6].

When the positron and electron spins are parallel, only spin-triplet Ps atoms are formed. On the other hand, when the spins are antiparallel, both spin-triplet and spin-singlet Ps atoms are formed. Therefore, by observing the change in the fraction of spin-triplet Ps or spin-singlet Ps upon spin reversal using spin-polarized positrons, information about the spin-polarized surface DOS may be obtained. Positrons emitted from radioisotopes are longitudinally spin polarized due to the parity nonconservation in the weak interaction. Hence, spin-polarized positron beams can be easily generated. Spin-polarized Ps spectroscopy may elucidate the nature of the spin polarization of the top-surface electronic states and play a valuable role in the field of spintronics.

Spin-polarized Ps spectroscopy was first demonstrated by the Michigan group in 1982 [7]. In their study, the spin polarization of a ferromagnetic Ni surface was determined from the field reversal asymmetry of the spin-triplet Ps fraction deduced from lifetime measurements. We demonstrated the feasibility of a similar experiment based on the energy spectra of annihilation $\gamma$ rays of spin-triplet Ps [8]. However, these existing methods cannot resolve the Ps kinetic energy, and hence the obtained spin polarization is only an average of all electrons below the Fermi level picked up by positrons. For more detailed analysis of the surface electronic states, determination of the electron spin polarization depending on the energy level, i.e., the spin-polarized DOS, is essential [9]. Spin-polarized and angle-resolved Ps spectroscopy with a submicron beam would be an ultimate surface spin probe that is applicable to device-scale samples.

In this work, we report on the development of a spin-polarized Ps time-of-flight (SP PsTOF) apparatus for the energy-resolved Ps spectroscopy. Using this apparatus, the Ps formation potentials for Pt, W, Ni, Co, $Co_2FeGa_{0.5}Ge_{0.5}$ (CFGG), and $Co_2MnSi$ (CMS) were successfully determined. Through the SP PsTOF experiments, we further examined the spin polarizations of the above ferromagnetic surfaces.

 

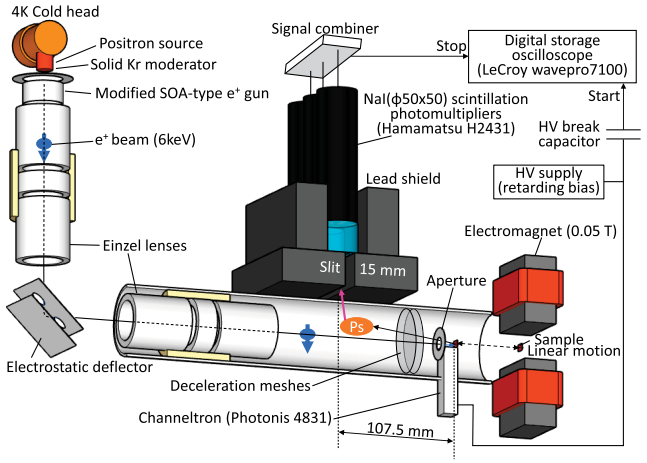


FIG. 1. Schematic diagram of the positronium time-of-flight apparatus developed in this work.

Figure 1 presents a schematic diagram of the SP PsTOF apparatus developed in this work. The $^{22}$Na source (162 MBq) was deposited on a graphite tray, which was inserted into a copper capsule equipped with a titanium window (5 $\mu$m thick) and a cone-shaped exit. The source capsule was mounted on a cold finger and cooled down to 4 K. A solid Kr moderator [10] was deposited on the surface of source exit. A slow positron beam was generated by a modified Soa gun [11] and transported using einzel lenses. A 90° electrostatic bending section was installed after the first einzel lens. Thereby, a transversely spin-polarized positron beam was obtained. The nominal beam energy was 6 keV. The beam diameter, flux, and spin polarization were approximately 5 mm, $10^4$ $e^+$/ sec, and 30%, respectively.

The positron beam was injected into the sample perpendicularly. The secondary electrons emitted upon positron impact were detected using a channeltron multiplier adjacent to the sample. This provided the start signal for the PsTOF measurement. The Ps atoms generated at the sample surface were ejected through an aperture of 20 mm diameter, which restricted the maximum emission angle to 22° with respect to the surface normal, and underwent annihilation during flight. The annihilation $\gamma$ rays were detected using three NaI scintillation detectors through lead slits. As spin-singlet Ps atoms promptly annihilate in the vicinity of the sample surface, this configuration permits detection of the annihilation events involving spin-triplet Ps atoms. In this way, PsTOF spectra were acquired.

The horizontal distance between the sample and the slit center was $L = 107.5$ mm. The slit width and length were $d = 15$ mm and $D = 50$ mm, respectively. The beam pipe radius was $R = 55$ mm, and hence the Ps atoms did not collide with the inner wall of the pipe prior to passing the slit section. Assuming that the Ps kinetic energy ($E_{\mathrm{Ps}}$) is monochromatic and Ps atoms are ejected with an angle of $\theta$ with respect to the surface normal, then the PsTOF spectrum has a distribution from time $t_1$ to $t_2$ given by

$$t_{1,2} = \frac{LD \mp d(D/2 + R)}{\sqrt{E_{\mathrm{Ps}}/m}(D\cos\theta \pm d\sin\theta)}, \tag{1}$$

where $m$ denotes the electron rest mass. Practically, $t_1$ represents the threshold time of the PsTOF spectrum, which is earlier than the ideal threshold time given by $d = 0$. The Ps atoms should also have a certain angular distribution reflecting the electron band dispersion relationship due to the momentum conservation law. Ps atoms emitted with larger $\theta$ values afford earlier $t_1$ values for the same $E_{\mathrm{Ps}}$. For the largest $\theta$ value of 22° using the present apparatus and the typical $E_{\mathrm{Ps}}$ value of 3 eV, $t_1 = 80$ ns, which is only 3 ns earlier than that for $\theta = 0°$. This was confirmed by a Monte Carlo simulation of the PsTOF spectrum considering the detection efficiency and time resolution of the electrical system, as depicted in Fig. 2(a). Figure 2(b) shows PsTOF spectra for various $E_{\mathrm{Ps}}$ values at $\theta = 0°$. These provide the total time resolution functions depending on $E_{\mathrm{Ps}}$. By converting the timescale to the energy scale, the energy resolution can be obtained (e.g., approximately 1 eV for $E_{\mathrm{Ps}} = 3$ eV). Practically, the energy resolution could be raised to 0.2–0.5 eV by optimizing the slit geometry.

Thus, even if we use the energy scale converted from the timescale with $E_{\mathrm{Ps}} = m(L'/t)^2$ and the effective length given by $L' = L - d(D/2 + R)/D$ for $\theta = 0°$, the error in the determination of the maximum Ps energy would be small. Ps atoms formed from electrons with wave vectors around the $\Gamma$ point and within $\theta \leq 22°$ are detected. The maximum transverse wave number of electrons picked up by positrons is given by $k_{\mathrm{max}} = 2\sqrt{m(-\Phi_{\mathrm{Ps}} + E)}\sin\theta/\hbar$, where $\Phi_{\mathrm{Ps}}$ is the Ps formation potential and $E$ is the electron

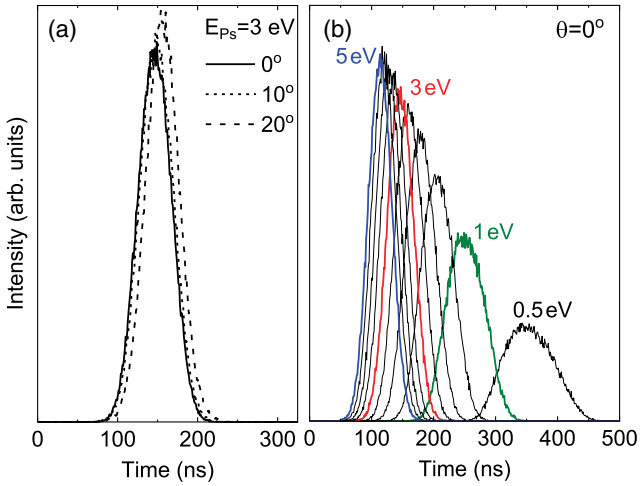


FIG. 2. Positronium time-of-flight spectra obtained via Monte Carlo simulations (a) for a positronium energy of 3 eV with various emission angles and (b) for an emission angle of 0° with positronium energies ranging from 0.5 to 5 eV in 0.5 eV steps.

energy (relative to the Fermi level $E_F$: $\Phi_{Ps} \leq E \leq 0$). For instance, for $\Phi_{Ps} = -3$ eV, $k_{max} \sim 0.5$ Å$^{-1}$ at $E_F$.

In the described apparatus, ferromagnetic samples could be in-plane magnetized using an electromagnet (50 mT) positioned in the sample preparation chamber. By rotating the sample around the beam center axis, the relative direction of positron spin polarization and magnetization could be varied from parallel to antiparallel. Different spectra under the parallel and antiparallel conditions would indicate the occurrence of polarization effects. The spin polarization of electrons depending on $E$ is given by

$$P_{-}^{\mathrm{TOF}}(E_{Ps}) = \frac{1}{P_{+}} \frac{2\epsilon(1) + \epsilon(0)}{2\epsilon(1) - \epsilon(0)} \frac{F_{\nparallel}(E_{Ps}) - F_{\parallel}(E_{Ps})}{F_{\nparallel}(E_{Ps}) + F_{\parallel}(E_{Ps})}, \quad (2)$$

where $F_{\parallel,\nparallel}(E_{Ps})$ denotes the PsTOF spectra obtained under the parallel-antiparallel spin conditions by converting the scale from time to energy with $E_{Ps} = -\Phi_{Ps} + E$, and $\epsilon(1) = 0.3$ and $\epsilon(0) = 0.4$ denote the detection efficiencies for annihilation $\gamma$ rays from Ps atoms with magnetic quantum numbers of $\pm 1$ and 0, respectively [12].

The samples used in this study were a mirror-polished W(001) bulk crystal, a Pt(111) film of 100 nm thickness grown on $Al_2O_3(0001)$ by magnetron sputtering deposition, Ni(111) and Co(0001) films of 30 nm thickness grown using an electron beam evaporator, and those covered with monolayer graphene grown via ultrahigh-vacuum chemical vapor deposition [13–15], CFGG(001) and CMS(001) films of 30 nm thickness grown on MgO(001) by magnetron sputtering deposition [16,17]. The samples were transferred through air into the sample chamber (base pressure: $10^{-8}$ Pa). The surfaces of the metal samples were cleaned via 1 keV Ar sputtering and subsequent heat treatment at appropriate temperatures. (The heat treatment temperatures for the CFGG and CMS samples were 800 and 400 °C, that maintain the $L2_1$ structure.) The surfaces of the graphene-covered Ni(111) and Co(0001) samples were cleaned by simply heating at 600 °C for 20 min.

To interpret the experimental data, density functional theory calculations were conducted using the ABINIT code [18] with the projector augmented wave method [19] within the generalized gradient approximation (GGA) [20]. The electron-positron correlation energy functional was based on the GGA method [21]. The initial valence electron configurations were assumed to be $5s^2 5p^6 5d^4 6s^2$ (W), $5s^2 5p^6 5d^9 6s^1$ (Pt), $3s^2 3p^6 3d^6 4s^1$ (Mn), $3s^2 3p^6 3d^7 4s^1$ (Fe), $3s^2 3p^6 3d^8 4s^1$ (Co), $3s^2 3p^6 3d^8 4s^2$ (Ni), $3d^{10} 4s^2 4p^1$ (Ga), $3d^{10} 4s^2 4p^2$ (Ge), $3s^2 3p^2$ (Si), and $2s^2 2p^2$ (C). For W and Pt, the spin-orbit interaction was also taken into consideration. The Ps formation potentials given by $\Phi_{Ps} = -A_{+} - 6.8$ eV, where $A_{+}$ is the positron affinity, were calculated using the bulk systems with primitive cells under full structural optimization. The $k$-point sampling was $10 \times 10 \times 10$. The spin-polarized surface electronic states of Co, Ni, CFGG, and CMS were calculated using film systems composed of seven monolayers stacked in the surface normal direction. For Co and Ni, the primitive cells were aligned parallel to the surfaces, while for CFGG and CMS, a conventional cell and two primitive cells, respectively, were aligned. In the calculation of graphene, C atoms were distributed on top of the Ni and Co surfaces. The van der Waals potential was also considered [22]. The vacuum layer was initially assumed to be 20 Å. Full structural optimization was also performed. The $k$-point sampling was $9 \times 9 \times 1$ for Fe, Co, and Ni, $5 \times 5 \times 1$ for CFGG and $12 \times 12 \times 1$ for CMS.

The surface DOS in the vacuum region, where Ps atoms may be formed, was computed from the ABINIT outputs. The region of $k$-point sampling was assumed to be $k \leq 2\sqrt{m(-\Phi_{Ps} + E)} \sin\theta/\hbar$. The electron-positron DOS ($D_{EP}$) was obtained by weighting the surface DOS with the positron density. Subsequently, the surface electron spin polarization depending on $E$ in the vacuum region was estimated as

$$P_{-}^{\mathrm{cal}}(E) = \frac{D_{EP}^{\uparrow}(E) - D_{EP}^{\downarrow}(E)}{D_{EP}^{\uparrow}(E) + D_{EP}^{\downarrow}(E)}, \quad (3)$$

where $\uparrow(\downarrow)$ denotes the majority (minority) spin channel. The details of the above calculations have been described elsewhere [8,23].

Figure 3 presents the PsTOF spectra obtained for the metal sample surfaces before and after subtracting the lifetime background of spin-triplet Ps [$\propto \exp(-t/142\ \mathrm{ns})$], as indicated by the broken curves. Approximately $5 \times 10^4$ annihilation events were accumulated for each spectrum. The peaks at $t = 0$ are attributable to prompt annihilation events, namely, the free annihilation of positrons in the samples and/or annihilation of spin-singlet Ps. The full width of the prompt peaks was approximately 70 ns. Upon closing the lead slits, these prompt peaks disappeared, which indicates that scattered $\gamma$ rays from the inner wall of the beam pipe were responsible for the prompt peaks. The spectrum threshold times were determined to be 35 ns later than the zero-cross points by considering the width of the prompt peaks mentioned above. From the maximum Ps kinetic energies given by the threshold times, the Ps formation potentials were determined to be −2.5 eV (Pt), −4.9 eV (W), −3.3 eV (Co), −2.7 eV (Ni), −3.9 eV (CFGG), and −4.8 eV (CMS). These values are in good agreement with the calculated Ps formation potentials (−2.8 eV (Pt), −5.2 eV (W), −3.6 eV (Co), −3.1 eV (Ni), −4.9 eV (CFGG) and −4.6 eV (CMS).

Figure 4 presents the spin polarizations [$P_{-}^{\mathrm{TOF}}(E_{Ps})$] as a function of Ps energy relative to the maximum value ($E_{Ps} + \Phi_{Ps}$) obtained from the SP PsTOF measurements and Eq. (2) for all the samples. In the cases of nonmagnetic Pt and W surfaces, only random and small fluctuations around zero are seen. For the Ni(111) and Co(0001) surfaces, the spin polarizations were negative from 0 eV

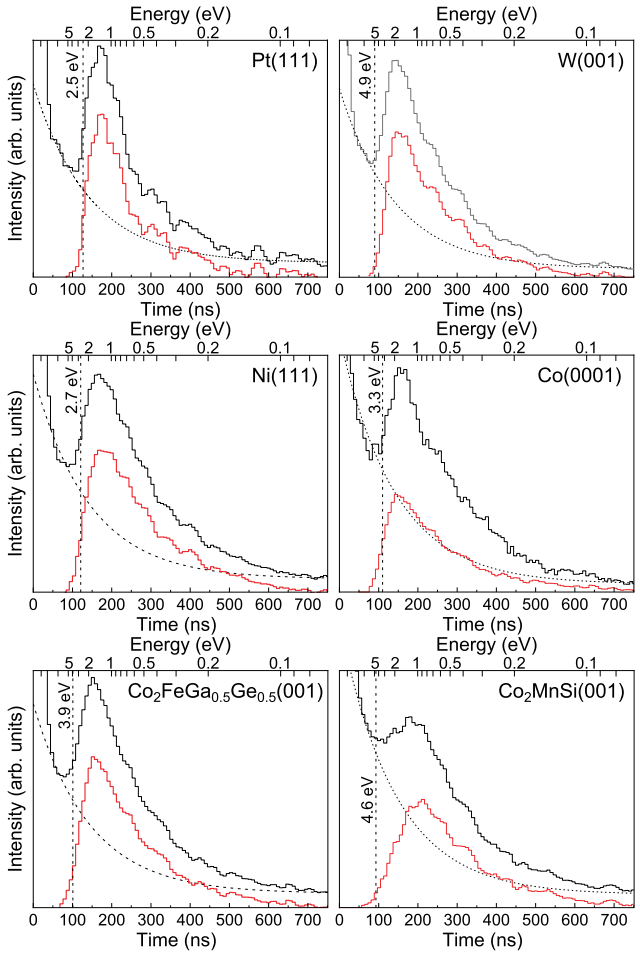


FIG. 3. Positronium time-of-flight spectra obtained for the Pt(111), W(001), Ni(111), Co,(0001), CFGG(001), and CMS(001) samples before and after subtracting the lifetime spectrum component of spin-triplet positronium (broken curves), i.e., $\propto \exp(-t/142\ \mathrm{ns})$. The chained lines indicate the positions of maximum positronium energies considering the time resolution of the measurement system.

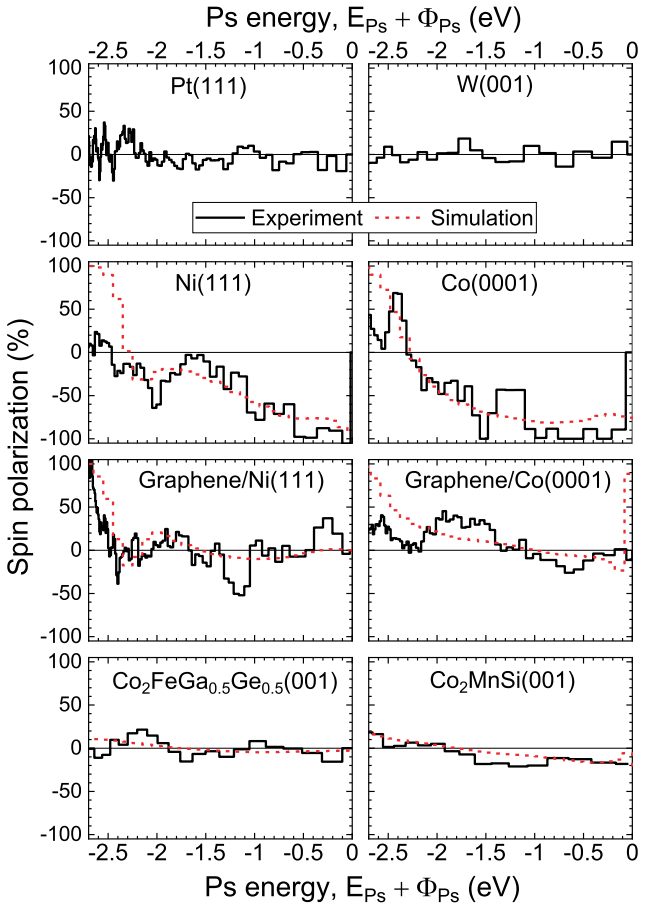


FIG. 4. Spin polarizations obtained from SP PsTOF measurements, $P_{-}^{\mathrm{TOF}}$, as a function of positronium energy relative to its maximum energy for the Pt(111), W(001), Ni(111), Co(0001), graphene/Ni(111), graphene/Co(0001), CFGG(001) and CMS(001) samples. The red broken curves represent the simulated spin polarization from the spin-polarized DOS ($D_{\mathrm{EP}}$) shown in Fig. 5 and the energy resolution function of PsTOF system.

to $-1.5 \sim -2$ eV. In contrast, for the graphene-covered Ni(111) and Co(0001) surfaces, the spin polarizations were sufficiently lost. The spin polarizations observed for the CFGG(001) and CMS(001) surfaces are also very small.

Figure 5 shows $D_{\mathrm{EP}}$ calculated for the Ni(111), Co(0001), graphene/Ni(111), graphene/Co(0001), CFGG(001), and CMS(001) surfaces. The surface of CFGG or CMS includes Co face and FeGaGe face or MnSi face equally. As seen from these plots, the spin polarization of the Ni(111) and Co(0001) surfaces in the vicinity of the Fermi level were negative. Whereas, the spin polarizations of the graphene-covered Ni(111) and Co(0001) surfaces were significantly lost near the Fermi level. The spin polarizations for the CFGG(001) and CMS(001) surfaces are also rather suppressed. (We discuss these details in the next paragraph.) For a direct comparison between the experimental and calculation results, Fig. 4 shows the SP PsTOF spectra simulated by convoluting $D_{\mathrm{EP}}$ with the system energy resolution function depending on the Ps energy (broken lines). These well reproduced the experimental data. This means that the experimental SP PsTOF spectrum shows the spin polarization below the Fermi level in an extended energy scale. For instance, the negative spin polarization of Ni down to $\sim -0.5$ eV in Fig. 5 is reflected down to $\sim -1.5$ eV in Fig. 4. Thus, the SP PsTOF measurement provides the spin polarization of topmost surface electrons around the $\Gamma$ point and near the Fermi level.

The spin polarizations of the Ni(111) and Co(0001) surfaces in the vicinity of the Fermi level are known to be negative owing to the *sd*-hybridized upper majority spin band with fewer states and the *d*-like upper minority spin band with more states [9,24]. In contrast, at the graphene/Ni(111) surface, the spin polarization has been reported to be positive on the basis of spin-polarized

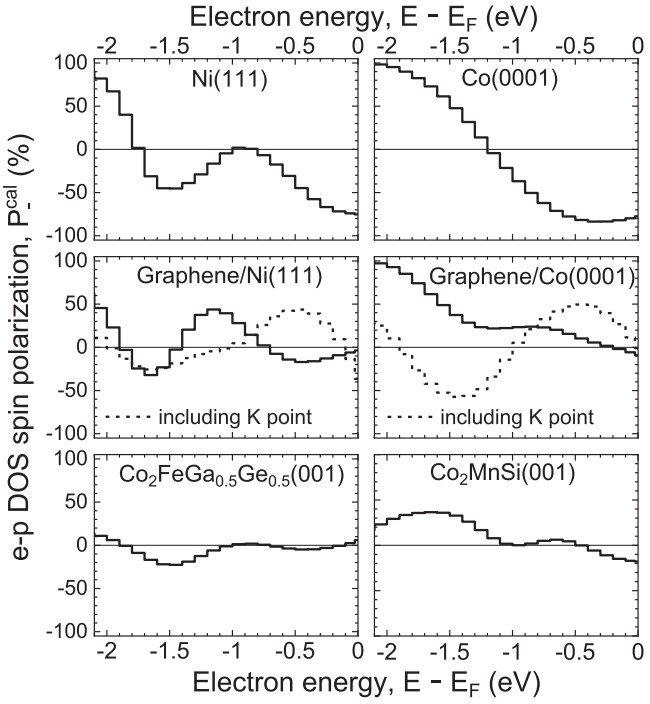


FIG. 5. Spin polarizations of electron-positron DOSs ($D_{EP}$) around the Γ point as a function of electron energy relative to the Fermi level calculated for Ni(111), Co(0001), graphene/Ni(111), graphene/Co(0001), CFGG(001) and CMS(001) surfaces. Broken lines represent the results including the $K$ point where the Dirac point of graphene is located.

metastable deexcitation spectroscopy results [25]. This has been explained via the polarization of the graphene DOS due to the strong hybridization of the graphene $\pi$ orbitals with the $dz^2$ and $dx^2 - y^2$ orbitals [26]. Hence, such a spin polarization should be induced near the $K$ point where the Dirac point of graphene is located. Actually, as shown in Fig. 5, the positive spin polarizations appear at around −0.5 eV in the calculation including $K$ points (broken lines). It is known that CFGG and CMS have half-metallic bulk characteristics. However, at the surfaces, the half-metallicity is not necessarily maintained. The present calculation indicates that the half-metallicity is lost even though important $k$ points related to the half-metallicity such as $X$ and $W$ points are sampled within the angle restriction. The reason for the absence of half-metallicity is explained as the formation of new surface bands in the gap of minority spin channel [27].

In this work, we demonstrated that the SP PsTOF spectroscopy provides the spin polarization of topmost surface electrons around the Γ point and near the Fermi level. There might be many potential applications of the current apparatus. For instance, the surface ferromagnetism predicted recently for narrow-gap semiconductors based on the quaternary Heusler alloys [28] is an intriguing target considering the fact that such a feature is absent in the conventional Heusler alloys. The angle-resolved Ps spectroscopy with a sufficient energy resolution has already been in use [6]. By extending this method to the spin-polarized version and furthermore by employing a sub-micron beam, the device-scale topological materials [29] in the ballistic conduction regime will also be attractive systems.

This work was financially supported by JSPS KAKENHI under Grants No. 17K19061 and No. 20K05454.

*Corresponding author.
kawasuso.atsuo@qst.go.jp

[1] A. P. Mills, L. Pfeiffer, and P. M. Platzman, Phys. Rev. Lett. **51**, 1085 (1983).
[2] A. Ishii, Solid State Phenom. **28&29**, 213 (1992).
[3] A. P. Mills, in *Positron Spectroscopy of Solids*, edited by A. Dupasquire and A. P. Mills (IOS Press, Ohmsha, Amsterdam, Oxford, Tokyo, Washington, DC, 1993), p. 209.
[4] A. Held and S. Kahana, Can. J. Phys. **42**, 1908 (1964).
[5] H. Kanazawa, Y. H. Ohtsuki, and S. Yanagawa, Phys. Rev. **138**, A1155 (1965).
[6] A. C. L. Jones, H. J. Rutbeck-Goldman, T. H. Hisakado, A. M. Pineiro, H. W. K. Tom, A. P. Mills, B. Barbiellini, and J. Kuriplach, Phys. Rev. Lett. **117**, 216402 (2016).
[7] D. W. Gidley, A. R. Köymen, and T. W. Capehart, Phys. Rev. Lett. **49**, 1779 (1982).
[8] A. Miyashita, M. Maekawa, K. Wada, A. Kawasuso, T. Watanabe, S. Entani, and S. Sakai, Phys. Rev. B **97**, 195405 (2018).
[9] I. I. Mazin, Phys. Rev. Lett. **83**, 1427 (1999).
[10] A. P. Mills, S. S. Voris, and T. S. Andrew, J. Appl. Phys. **76**, 2556 (1994).
[11] K. F. Canter, P. H. Lippel, W. S. Crane, and A. P. Mills, in *Positron Studies of Solids, Surfaces, and Atoms*, edited by A. P. Mills, W. S. Crane, and K. Canter (World Scientific, Singapore, 1986), p. 199.
[12] R. M. Drisko, Phys. Rev. **102**, 1542 (1956).
[13] S. Entani, Y. Matsumoto, M. Ohtomo, P. V. Avramov, H. Naramoto, and S. Sakai, J. Appl. Phys. **111**, 064324 (2012).
[14] Y. Matsumoto, S. Entani, A. Koide, M. Ohtomo, P. V. Avramov, H. Naramoto, K. Amemiya, T. Fujikawa, and S. Sakaia, J. Mater. Chem. C **1**, 5533 (2013).
[15] M. Ohtomo, Y. Yamauchi, A. A. Kuzubov, N. S. Eliseeva, P. V. Avramov, S. Entani, Y. Matsumoto, H. Naramoto, and S. Sakai, Appl. Phys. Lett. **104**, 051604 (2014).
[16] S. Li, K. V. Larionov, Z. I. Popov, T. Watanabe, K. Amemiya, S. Entani, P. V. Avramov, Y. Sakuraba, H. Naramoto, P. B. Sorokin, and S. Sakai, Adv. Mater. **32**, 1905734 (2020).
[17] Y. Sakuraba, M. Hattori, M. Oogane, Y. Ando, H. Kato, A. Sakuma, T. Miyazaki, and H. Kubota, Appl. Phys. Lett. **88**, 192508 (2006).
[18] X. Gonze, J.-M. Beuken, R. Caracas, F. Detraux, M. Fuchs, G.-M. Rignanese, L. Sindic, M. Verstraete, G. Zerah, F. Jollet, M. Torrent, A. Roy, M. Mikami, P. Ghosez, J.-Y. Raty, and D. Allan, Comput. Mater. Sci. **25**, 478 (2002).
[19] P. E. Blöchl, Phys. Rev. B **50**, 17953 (1994).

[20] J. P. Perdew, K. Burke, and M. Ernzerhof, Phys. Rev. Lett. **77**, 3865 (1996).
[21] B. Barbiellini and J. Kuriplach, Phys. Rev. Lett. **114**, 147401 (2015).
[22] S. Grimme, J. Comput. Chem. **27**, 1787 (2006).
[23] A. Kawasuso, M. Maekawa, A. Miyashita, K. Wada, T. Kaiwa, and Y. Nagashima, Phys. Rev. B **97**, 245303 (2018).
[24] S. Wakoh, J. Phys. Soc. Jpn. **20**, 1894 (1965).
[25] S. Entani, M. Kurahashi, X. Sun, and Y. Yamauchi, Carbon **61**, 134 (2013).
[26] X. Sun, S. Entani, Y. Yamauchi, A. Pratt, and M. Kurahashi, J. Appl. Phys. **114**, 143713 (2013).
[27] S. J. Hashemifar, P. Kratzer, and M. Scheffler, Phys. Rev. Lett. **94**, 096402 (2005).
[28] S. Keshavarz, I. DiMarco, D. Thonig, L. Chioncel, O. Eriksson, and Y. O. Kvashnin, Phys. Rev. Mater. **4**, 021401(R) (2020).
[29] N. P. Armitage, E. J. Mele, and A. Vishwanath, Rev. Mod. Phys. **90**, 015001 (2018).